Reaction Kinetics of $CO + HO_2 \rightarrow$ Products: Ab Initio Transition State Theory Study with Master Equation Modeling†

Xiaoqing You and Hai Wang*

Department of Aerospace and Mechanical Engineering, University of Southern California, Los Angeles, California 90089

Elke Goos

Institute of Combustion Technology, DLR, Pfaffenwaldring 38, 70569 Stuttgart, Germany

Chih-Jen Sung

Department of Mechanical and Aerospace Engineering, Case Western Reserve University, Cleveland, Ohio 44106

Stephen J. Klippenstein*

Chemistry Division, Argonne National Laboratory, Argonne, Illinois 60439

Received: November 15, 2006; In Final Form: January 18, 2007

The kinetics of the reaction $CO + HO_2\bullet \rightarrow CO_2 + \bullet OH$ was studied using a combination of ab initio electronic structure theory, transition state theory, and master equation modeling. The potential energy surface was examined with the CCSD(T) and CASPT2 methods. The classical energy barriers were found to be about 18 and 19 kcal/mol for $CO + HO_2\bullet$ addition following the trans and cis paths, respectively. For the cis path, rate constant calculations were carried out with canonical transition state theory. For the trans path, master equation modeling was also employed to examine the pressure dependence. Special attention was paid to the hindered internal rotations of the HOOC•O adduct and transition states. The theoretical analysis shows that the overall rate coefficient is independent of pressure up to 500 atm for temperature ranging from 300 to 2500 K. On the basis of this analysis, we recommend the following rate expression for reaction R1 $k(\mathrm{cm^3/mol\cdot s}) = 1.57 \times 10^5\, T^{2.18} \mathrm{e}^{-9030/T}$ for $300 \le T \le 2500$ K with the uncertainty factor equal to 8, 2, and 1.7 at temperatures of 300, 1000, and 2000 K, respectively.

Introduction

Recent interest in the reaction kinetics of

$$CO + HO_2\bullet \rightarrow CO_2 + \bullet OH \qquad \text{(R1)}$$

stems from its influence on the oxidation rate of CO and H_2 mixtures at high pressures.[1−3] Although extensive experimental studies have been reported,[4−23] large discrepancies exist among literature rate values over the temperature range of interest to combustion kinetics, as seen in Figure 1. Above the temperature of 500 K, all measurements are either indirect or the rate coefficient values were inferred from kinetic measurements on reaction processes in which reaction R1 is of secondary importance. Below 500 K, a few direct measurements are available; all of them yield only an upper limit for the rate coefficient. Hence, these studies provide little to no quantitative guidance for the rate coefficient above 500 K.

Among measurements made above 500 K, Baldwin and coworkers[4,6,16] studied k_1 relative to the reaction

$$HO_2\bullet + HO_2\bullet \rightarrow H_2O_2 + O_2 \qquad \text{(R2)}$$

in a static reactor. They obtained $k_1/\sqrt{k_2} = 13.4 \pm 0.05$ $(\mathrm{cm^3/mol\cdot s})^{1/2}$, and based on an obsolete k_2 value, they recommended $k_1 = 1.9 \times 10^7$ $\mathrm{cm^3/mol\cdot s}$ at 773 K.[16] Mueller et al.[31] reinterpreted the rate data by taking k_2 from Hippler et al.[33] and obtained $k_1 = 1 \times 10^7$ $\mathrm{cm^3/mol\cdot s}$. On the basis of this rate value, Mueller et al.[31] recommended

$$k_1(\mathrm{cm^3/mol\cdot s}) = 3 \times 10^{13}\mathrm{e}^{-11575/T} \qquad \text{for } 750 \le T \le 1100 \text{ K}$$

The rate expression has been used extensively in subsequent combustion kinetics studies. Other rate expressions that have been used include that of Tsang and Hampson[30]

$$k_1(\mathrm{cm^3/mol\cdot s}) = 1.5 \times 10^{14}\mathrm{e}^{-11900/T} \qquad \text{for } 700 \le T \le 1000 \text{ K}$$

The above rate expression is based on a wider range of experimental data and is about a factor of 3 larger than that of Mueller et al. The discrepancies of the two rate expressions given above are, however, well within the uncertainties of each other.

Very recently, Mittal et al.[1] carried out an autoignition study of H_2/CO mixtures in the temperature range of 950−1100 K and pressures from 15 to 50 bar in a rapid compression machine

† Part of the special issue "James A. Miller Festschrift".

* Corresponding authors. E-mail: haiw@usc.edu; sjk@anl.gov.

10.1021/jp067597a CCC: $37.00
Published on Web 03/22/2007

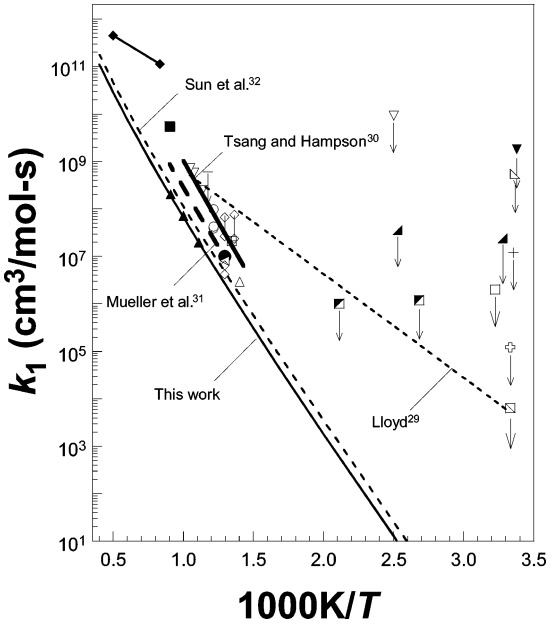

Figure 1. Arrhenius plot of k_1. Symbols: experimental data (left-pointing triangle): Baldwin et al.,[4] based on $k_1/\sqrt{k_{ref}}$ measurements relative to $HO_2\bullet + HO_2\bullet = H_2O_2 + O_2$ (R2) (k_{ref} taken from Kappel et al.[24]) and $HO_2\bullet + H_2 = H_2O_2 + H\bullet$ (k_{ref} taken from Baulch et al.[25]); ◇: Hoare and Patel,[5] based on measurements relative to $C_2H_6 + HO_2\bullet \rightarrow C_2H_5\bullet + H_2O_2$ (k_{ref} based on Baldwin et al.[26] and also from Kappel et al.[24]) and to $C_2H_4 + HO_2\bullet \rightarrow$ products (k_{ref} taken from Baulch et al.[25]); △: Baldwin et al.,[6] based on $k_1/\sqrt{k_{ref}}$ measurements relative to reaction 2 (k_{ref} taken from Kappel et al.[24]) −: Azatyan;[7] (open right triangle): Volman and Gorse,[8] based on measurements relative to $CO + OH\bullet \rightarrow CO_2 + H\bullet$ (k_{ref} taken from Joshi and Wang[27]); ⊞: Khachatrian et al.;[10] ⧅: Davis et al.,[11] based on $k_1/\sqrt{k_{ref}}$ measurements relative to reaction 2 (k_{ref} taken from Atkinson et al.[28]); ◩: Simonaitis and Heicklen,[12] based on $k_1/\sqrt{k_{ref}}$ measurements relative to reaction 2 (k_{ref} taken from Atkinson et al.[28]); □: Wyrsch et al.;[13] ▽: Hastie,[14] based on measurements relative to $CO + OH\bullet \rightarrow CO_2 + H\bullet$ (k_{ref} taken from Joshi and Wang[27]); ▽: Vardanyan et al.;[15] ●: Atri et al.,[16] based on $k_1/\sqrt{k_{ref}}$measurements relative to reaction 2 (k_{ref} taken from Kappel et al.[24]) ■: Colket et al.;[17] (open cross): Graham et al.;[18] +: Burrow et al.;[19] (solid right triangle): Howard;[20] ○: Arustamyan et al.[21] re-evaluated in the present work, using the rate coefficient values of $OH\bullet + H_2 \rightarrow H_2O + H\bullet$ and $CO + OH\bullet \rightarrow CO_2 + H\bullet$ from Baulch et al.[25] and Joshi and Wang,[27] respectively; ♦: Vandooren et al.;[22] ▼: Bohn and Zetsch;[23] ▲: Mittal et al.[1] Lines: selected compilations and theoretical studies. Arrows indicate that the rate values are upper limits.

(RCM). They noted that the reproduction of their experimental data requires k_1 values that are notably smaller than those previously understood. On the basis of the prediction of onset of ignition and sensitivity analyses, Mittal et al.[1] recommended that

$$k_1(\text{cm}^3/\text{mol}\cdot\text{s}) = 7.5 \times 10^{12} e^{-11575/T}$$

At 1000 K, the above expression gives $k_1 = 7 \times 10^7$ cm^3/mol·s, as much as a factor of 4 smaller than that of Mueller et al.[31] The rate coefficient given in ref 1 is also outside of the uncertainties of previously reported values (see Figure 1). A follow-up study by Mittal et al.[2] used "Morris-one-at-a-time" and Monte Carlo uncertainty analyses. The results again pointed to a much lower value for k_1 than those from previous experimental studies and evaluations.

Around 1000 K, there have been several experimental studies reported for reaction R1, all of which were based on indirect measurements. In all cases, the k_1 values reported are substantially larger than what was needed to explain the RCM data. Colket et al.[17] estimated the value of k_1 from the rate of CO_2 formation in acetaldehyde oxidation for temperatures between 1030 and 1150 K, obtaining a k_1 value that is over an order of magnitude larger than that of Mittal et al.[1] These experiments might have been influenced by impurities present in the acetaldehyde.[31,34] Vardanyan et al.[15] measured the CO_2 production in a CH_2O flame in the temperature range of 878−952 K. The concentration of $HO_2\bullet$ radicals was estimated by freezing out the free radicals and analyzing them with electron spin resonance. On the basis of these measurements, a k_1 value of 7×10^8 cm^3/mol·s was reported for $T = 952$ K. Using a similar approach, Arustamyan et al.[21] studied the slow oxidation of CO in the presence of H_2 in a flow system for temperatures of 803−843 K and pressures of 300−530 Torr. By following the CO_2 production rate, a k_1 value of 1.1×10^8 cm^3/mol·s may be obtained from the modeling of the overall reaction process. The only experiment that produced a rate value close to that of Mittal et al.[1] was that of Hoare and Patel,[5] who measured k_1 relative to

$$C_2H_6 + HO_2\bullet \rightarrow C_2H_5\bullet + H_2O_2 \qquad \text{(R3)}$$

$$C_2H_4 + HO_2\bullet \rightarrow \text{products} \qquad \text{(R4)}$$

at temperatures between 734 and 773 K. Unfortunately, neither k_3 nor k_4 is accurately known, and the resulting k_1 value is still highly uncertain.

Reaction R1 has also been the subject of a few theoretical studies. Allen et al.[35] carried out single-point CISD calculations at geometries optimized at the HF/6-31G(d) level of theory. On the basis of the potential energy surface, they proposed that the reaction proceeds through a chemically activated path via the *trans*-HOOC•O adduct:

$$CO + HO_2\bullet \rightarrow [\textit{trans}\text{-HOOC}\bullet\text{O}]^* \rightarrow CO_2 + \bullet OH \qquad \text{(R1′)}$$

The ground state of the adduct was predicted to be a shallow well, lying 11.6 kcal/mol above the entrance channel, and with critical energies of only 11 and 7 kcal/mol for dissociation into $CO + HO_2\bullet$ and $CO_2 + OH\bullet$, respectively. The shallowness of the well suggests that the discrepancy in k_1 between Mittal et al.[1] and earlier measurements cannot be attributed to its pressure dependency because collisional stabilization of the adduct is expected to be inefficient for pressures up to several hundred atmospheres. Very recently, Sun et al.[32] computed k_1 using canonical transition state theory based on G3MP2 energies and optimized MP2(full)/6-31G(d,p) geometries. They considered only the trans conformer pathway, as did Hsu et al.,[36] and presented a theoretical expression for k_1 of

$$k_1(\text{cm}^3/\text{mol}\cdot\text{s}) = 1.15 \times 10^5 T^{2.28} e^{-8830/T}$$

$$\text{for } 300 \le T \le 2500 \text{ K}$$

Within the temperature range of 950−1100 K, this theoretical rate coefficient is well within a factor of 2 of the rate coefficient obtained from the RCM experiment. Unfortunately, these prior theoretical efforts are insufficient to ensure an accurate rate coefficient. In all cases, the hindered internal rotations in the HOOC•O adduct and the critical geometries were treated inadequately; and the complexity of the potential energy surface due to the trans and cis conformers and their mutual isomerization was not considered. In addition, the calculations of the potential energy barriers may not be sufficiently reliable to obtain accurate k_1 values.

The purpose of the present study is to provide an improved theoretical treatment of reaction R1. This treatment includes a more detailed analysis of the potential energy surface of reaction R1 using several high-level quantum chemistry methods. Our best estimates for the saddle point energies are then incorporated in transition state theory simulations that consider the full complexity of the hindered rotational motions. Furthermore, the possibility of collisional stabilization and the dissociation of the adduct back to CO + HO_2• along the trans pathway is examined via master equation simulations.

Computational Details

Potential Energy Surface. The geometries and vibrational frequencies for all of the stationary points considered here were obtained from coupled cluster theory with single and double excitations, including perturbational estimates of the effects of the connected triple excitations, CCSD(T), and employing Dunning's correlation-consistent cc-pVTZ basis sets.[37] Additional single-point calculations were performed at the CCSD(T)/cc-pVQZ level of theory and the CCSD(T)/cc-pVTZ geometries. The results of G3B3 calculations are also reported here for comparison. All of the CCSD(T) and G3B3 ab initio calculations were carried out using the Gaussian 03 program package.[38]

Basis set extrapolation was carried out following the method of Halkier et al.[39]

$$E_{\mathrm{CCSD(T)}}(X) \approx E_{\mathrm{CCSD(T)}}(\infty) + aX^{-3} \quad (1)$$

where $E_{\mathrm{CCSD(T)}}(X)$ and $E_{\mathrm{CCSD(T)}}(\infty)$ are the CCSD(T) energies with the cc-pVXZ basis set and at the CBS limit, respectively. The basis sets cc-pVDZ, cc-pVTZ, and cc-pVQZ have $X = 2$, 3, and 4, respectively. The resulting CCSD(T)/CBS energy is

$$E_{\mathrm{CCSD(T)/CBS}} \approx E_{\mathrm{CCSD(T)/cc-pVQZ}} + \frac{27}{37} \times [E_{\mathrm{CCSD(T)/cc-pVQZ}} - E_{\mathrm{CCSD(T)/cc-pVTZ}}] \quad (2)$$

where $E_{\mathrm{CCSD(T)/cc-pVQZ}}$ is the single-point energy at the CCSD(T)/cc-pVTZ geometry. In addition to basis set extrapolation, we also made an approximate correction for the CI truncation error using the somewhat empirical scaling method proposed by He et al.[40] The same method was adopted by Yu et al.[41] in their study of CO + •OH = CO_2 + H•. Let $E^{T}_{\mathrm{CCSD(T)/cc-pVTZ}}$ be the perturbation energy of the connected triple excitations at the CCSD(T)/cc-pVTZ level of theory. The CI truncation error may be estimated to be 20−25% of $E^{T}_{\mathrm{CCSD(T)/cc-pVTZ}} = E_{\mathrm{CCSD(T)/cc-pVTZ}} - E_{\mathrm{CCSD/cc-pVTZ}}$.[40] Therefore, the full coupled cluster/complete basis set (FCC/CBS) energy may be estimated as

$$E_{\mathrm{FCC/CBS}} \approx E_{\mathrm{CCSD(T)/cc-pVQZ}} + \frac{27}{37} \times [E_{\mathrm{CCSD(T)/cc-pVQZ}} - E_{\mathrm{CCSD(T)/cc-pVTZ}}] + \frac{1}{5}E^{\mathrm{T}}_{\mathrm{CCSD(T)/cc-pVTZ}} \quad (3)$$

During the course of the study, it was found that the T1 diagnostic of our CCSD(T) calculation is modestly larger than 0.02 for the two key transition states (TS1 following the trans pathway and TS3 following the cis pathway of CO + HO_2• addition, as described below). This finding casts some doubt on the reliability of single-reference-based CCSD(T) correlation treatments for these transition states.[42,43] For this reason, internally contracted multireference CASPT2[44] and configuration interaction (MRCI) calculations with single and double excitations were also carried out, with the goal of delineating the uncertainty of the energy barriers for such cases. These calculations focused on TS1 because similar results are expected for the closely related TS3. For these calculations, the geometry was optimized with a five electron five orbital (5e,5o) CASPT2 calculation employing Dunning's correlation-consistent aug-cc-pVTZ basis set. The five active orbitals in this calculation correlate with the π and π* orbitals of CO and the radical orbital of HO_2• (i.e., the O_2 π* orbital). Single-point calculations at these geometries were performed with 9 electron 8 orbital (9e,8o), and 11 electron 10 orbital active spaces (11e,10o). The (9e,8o) active space included the O_2 π, $p\sigma$, and $p\sigma$* orbitals of the HO_2 component. The (11e,10o) space added the CO $p\sigma$ and $p\sigma$* orbitals to the (9e,8o) active space. These CASPT2 and MRCI calculations were performed with the MOLPRO software package.[45]

Reaction Rate Coefficients. Rate coefficients were calculated using a Monte Carlo code for the solution of the master equation of the collision energy transfer, as reported previously.[27] Briefly, for the reaction path through the *trans*-HOOC•O adduct, the time evolution of a rovibrationally excited molecule is described by the master equation in discrete form

$$\frac{\mathrm{d[A}(E_i)]}{\mathrm{d}t} = \sum_j k_{ij}[\mathrm{M}][\mathrm{A}(E_j)] - \sum_i k_{ji}[\mathrm{M}][\mathrm{A}(E_i)] - \sum_m k_m(E_i)[\mathrm{A}(E_i)] \quad (4)$$

where [A(E_i)] denotes the concentration of species A at the energy state E_i; [M] is the concentration of bath-gas molecules; k_{ij} is the rate constant for the collision energy transfer from energy state j to state i, and $k_m(E_i)$ is the microcanonical rate constant for the mth channel, which also accounts for the dissociation of the adduct back to CO + HO_2•. In this formulation, the bimolecular rate coefficient of CO + HO_2• is handled by the equilibrium constant of CO + HO_2• addition. The collisional energy transfer probability was described by the exponential down model, with $\langle \Delta E_{\mathrm{down}} \rangle = 260$ cm^{-1}. Because of the shallow potential energy well, the stabilization of the adduct is minimal and the computed k_1 value was insensitive to the $\langle \Delta E_{\mathrm{down}} \rangle$ value. Monte Carlo simulations used an energy grain size equal to 10 cm^{-1}, as in a previous study.[27]

For the cis pathway, it will be shown that a potential energy minimum does not exist along the reaction path, and, as such, its contribution to the overall rate is calculated with conventional transition state theory

$$k = \frac{k_{\mathrm{B}}T}{h}\frac{Q_{\mathrm{TS}}}{Q_{\mathrm{reac}}}\,\mathrm{e}^{-E_0/R_{\mathrm{u}}T} \quad (5)$$

where k_{B} is Boltzmann's constant, h is Planck's constant, Q is the total partition function, E_0 is the energy barrier, and R_{u} is the universal gas constant.

Hindered Internal Rotation. There are two hindered rotors in the HOOC•O adduct and in the transition states associated with the adduct: about the HOO−C•O bond and the HO−OC•O bond. The HOO−C•O internal rotation is responsible for the mutual isomerization of the trans and cis conformers along the reaction path. Both hindered rotors are expected to influence the partition functions of the internal degrees of freedom. Here the energy barriers for these hindered internal rotors were examined at the B3LYP/6-31G(d) and CCSD(T)/cc-pVTZ levels of theory. Moments of inertia were estimated using several approaches, following East and Radom.[46] Here the various

approximations are denoted as $I^{(m,n)}$ for moment of inertia or $B^{(m,n)}$ for the rotational constant, where n denotes the level of approximation for a rotor attached to a fixed frame due to coupling with external or other internal rotation and m indicates the level of approximation of the coupling reduction. At a lower level of approximation, the moment of inertia may be given as

$$I^{(2,n)} = \frac{I_L^{(1,n)} I_R^{(1,n)}}{I_L^{(1,n)} + I_R^{(1,n)}} \tag{6}$$

where subscript L and R indicate the "left" and "right" rotating group of the twisting bond, respectively. For $n = 1$, the moment of inertia is calculated by assuming the rotational axis to be the twisting bond; and for $n = 2$, the axis is assumed to be parallel to the twisting bond but passing through the center of mass of the rotating group. For $n = 3$, the axis passes through the centers of mass of both the rotating groups and the remainder of the molecule. These approximations have been used extensively in previous theoretical rate studies (see, e.g., ref 47).

During the course of our study, we found that the theoretical k_1 value was quite sensitive to the approximations made for the moments of inertia of the hindered internal rotors. For this reason, they were treated with some care by considering fully the coupling with external rotation.[46,48] In this approach, we define two coordinate systems. The first (x,y,z) is attached to one of the two rotating moieties; and the second is associated with the principal axes of external rotation (1,2,3). It may be shown that the moment of inertia is independent of the choice of the moiety ("left" or "right") selected for the (x,y,z) coordinates.[46] The z axis is the twisting bond, and the x axis passes through the center of mass of a rotating moiety. The axes of the rotating moiety (x,y,z) and the axes of the parent molecule are both right-handed with α_{ix}, α_{iy}, and α_{iz} being the direction cosines between the two sets of coordinates, where i = 1, 2, and 3 for principal axes 1, 2, and 3, respectively. The moment of inertia is given by

$$I^{(3,4)} = I^{(1,1)} - \sum_{i=1}^{3}\left[\frac{(\alpha_{iy}U)^2}{m_L + m_R} + \frac{\beta_i^2}{I_i}\right] \tag{7}$$

where $I^{(1,1)}$ is the moment of inertia about the z axis

$$I^{(1,1)} = \sum_{j\in \text{L or R}} m_j(x_j^2 + y_j^2) \tag{8}$$

m_j is the mass of the jth atom, and x_j and y_j are the position of the jth atom in the (x,y,z) coordinates. In eq 7, U is the off-balance factor, given by

$$U = \sum_{j\in \text{L or R}} m_j x_j \tag{9}$$

β_i is given by

$$\beta_i = \alpha_{iz} I^{(1,1)} - \alpha_{ix} C - \alpha_{iy} D + U(\alpha_{i-1,y} r_{i+1} - \alpha_{i+1,y} r_{i-1}) \tag{10}$$

where the subscripts $i - 1$ and $i + 1$ refer to cyclic shifts of axes so that $i - 1 = 3$ if $i = 1$, and $i + 1 = 1$ if $i = 3$, r_i is the distance along the ith coordinate from the center of mass of the parent molecule to the origin of coordinates of the rotating moiety; and C and D are the cross products, which are given, respectively, by

$$C = \sum_{j\in \text{L or R}} m_j x_j z_j \tag{11}$$

$$D = \sum_{j\in \text{L or R}} m_j y_j z_j \tag{12}$$

For the current calculation, we consider the nonsymmetric nature of the hindered internal rotations in HOOC•O and its transition states. Specifically, the two potential energy wells following a full internal rotation are assumed to be asymmetric about the minima (see, Figure 2). We express the potential energy in four separate parts:

$$V(\phi) = \begin{cases} \left(\frac{V_{01}}{2}\right)[1 - \cos(2\phi)] & 0 \le \phi < \pi/2 \\ \left(\frac{V_{02}}{2}\right)[1 - \cos(2\phi)] + (V_{01} - V_{02}) & \pi/2 \le \phi < \pi \\ \left(\frac{V_{03}}{2}\right)[1 - \cos(2\phi)] + (V_{01} - V_{02}) & \pi \le \phi < 3\pi/2 \\ \left(\frac{V_{04}}{2}\right)[1 - \cos(2\phi)] & 3\pi/2 \le \phi < 2\pi \end{cases} \tag{13}$$

where ϕ is the rotation angle. Obviously, the four potential energy barriers are bound by the relation $V_{03} = V_{04} - (V_{01} - V_{02})$. The classical partition function of a one-dimensional hindered rotor for the above potential function may be written as

$$Q_h(T) = \frac{1}{2\pi}\left(\frac{\pi k_B T}{B}\right)^{1/2} \sum_{i=1}^{4} \int_{(i-1)\pi/2}^{i\pi/2} d\phi e^{-V/k_B T} = \frac{Q_f(T)}{4} \sum_{i=1}^{4} \exp\left[-\frac{V_{0i} + 2\delta_i(V_{01} - V_{02})}{2k_B T}\right] \mathbf{I}_0\left(\frac{V_{0i}}{2k_B T}\right) \tag{14}$$

where $\delta_i = 0$ for $i = 1$ and 4, and $\delta_i = 1$ for $i = 2$ and 3, B is the rotational constant, Q_f is the partition function in the limit of a free rotor, and $\mathbf{I}_0(\ )$ is the modified Bessel function. The density of energy states for a full 2π internal rotation is a sum of contributions from the four parts of the potential function

$$\rho_h(E) = \rho_{h1}(E) + \rho_{h2}(E) + \rho_{h3}(E) + \rho_{h4}(E) \tag{15}$$

where

$$\rho_{h1}(E) = \begin{cases} \dfrac{\mathbf{K}\left(\sqrt{\frac{E}{V_{01}}}\right)}{2\pi\sqrt{BV_{01}}} & \text{for } 0 < E < V_{01} \\ \dfrac{\mathbf{K}\left(\sqrt{\frac{V_{01}}{E}}\right)}{2\pi\sqrt{BE}} & \text{for } E > V_{01} \end{cases}$$

$$\rho_{h4}(E) = \begin{cases} \dfrac{\mathbf{K}\left(\sqrt{\frac{E}{V_{04}}}\right)}{2\pi\sqrt{BV_{04}}} & \text{for } 0 < E < V_{04} \\ \dfrac{\mathbf{K}\left(\sqrt{\frac{V_{04}}{E}}\right)}{2\pi\sqrt{BE}} & \text{for } E > V_{04} \end{cases}$$

$$\rho_{h2}(E) = \begin{cases} \dfrac{\mathbf{K}\left(\sqrt{\dfrac{E-(V_{01}-V_{02})}{V_{02}}}\right)}{2\pi\sqrt{BV_{02}}} & \text{for } 0 < E-(V_{01}-V_{02}) < V_{02} \\ \dfrac{\mathbf{K}\left(\sqrt{\dfrac{V_{02}}{E-(V_{01}-V_{02})}}\right)}{2\pi\sqrt{B[E-(V_{01}-V_{02})]}} & \text{for } E-(V_{01}-V_{02}) > V_{02} \end{cases}$$

$$\rho_{h3}(E) = \begin{cases} \dfrac{\mathbf{K}\left(\sqrt{\dfrac{E-(V_{01}-V_{02})}{V_{03}}}\right)}{2\pi\sqrt{BV_{03}}} & \text{for } 0 < E-(V_{01}-V_{02}) < V_{03} \\ \dfrac{\mathbf{K}\left(\sqrt{\dfrac{V_{03}}{E-(V_{01}-V_{02})}}\right)}{2\pi\sqrt{B[E-(V_{01}-V_{02})]}} & \text{for } E-(V_{01}-V_{02}) > V_{03} \end{cases}$$

where E is the energy relative to the lower one of the two potential energy wells and $\mathbf{K}(\,)$ is the complete elliptic integral of the first kind. In eq 15, the four terms correspond to rotations with $0 < \phi < \pi/2$, $\pi/2 < \phi < \pi$, $\pi < \phi < 3\pi/2$, and $3\pi/2 < \phi < 2\pi$, respectively.

Because of the unique potential energy surface to be discussed later, there is a need to treat the trans and cis conformers separately along the reaction coordinates. Because each of the two potential energy wells illustrated in Figure 2 corresponds to a particular conformer, eq 15 may be reduced to only two terms to give the hindered rotation contribution from a particular conformer, as will be discussed later.

The total density of states can be obtained by the convolution procedure[49,50]

$$\rho(E) = \int_0^E \rho_h(E)\rho_{nh}(E-e)de \qquad (16)$$

where ρ_{nh} is the density of states for degrees of freedom other than the hindered rotors. The sum of states is calculated by integrating $\rho(E)$

$$W(E) = \int_0^E \rho(e)de \qquad (17)$$

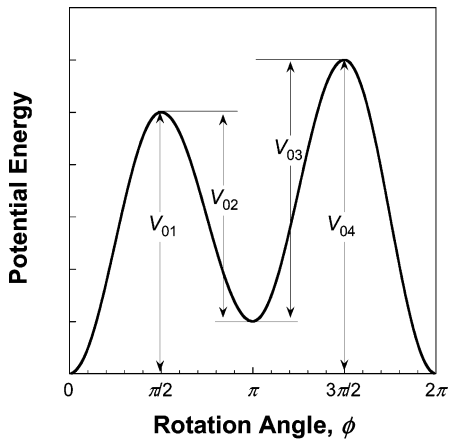

Figure 2. Schematic illustration of the potential energy function for the asymmetric, hindered internal rotation.

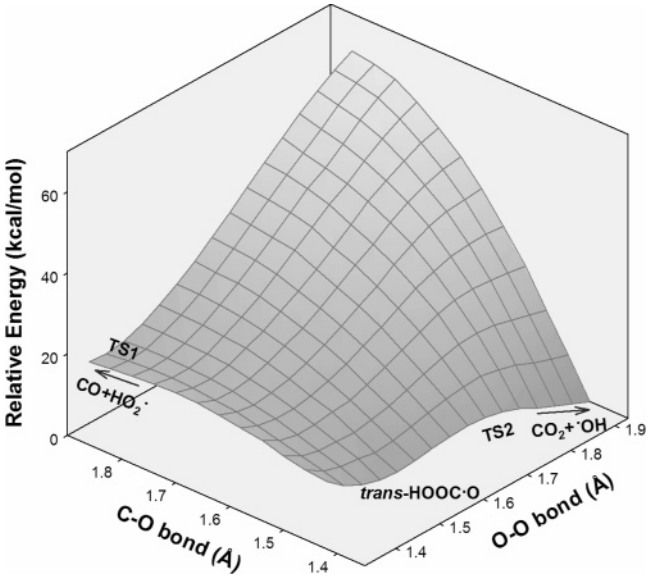

Figure 3. Relaxed potential energy scan for $(CO + HO_2\bullet) \rightarrow$ TS1 $\rightarrow$ *trans*-HOOC•O $\rightarrow$ TS2 $\rightarrow (CO_2 + \bullet OH)$ at the B3LYP/6-31G(d) level of theory without zero-point correction.

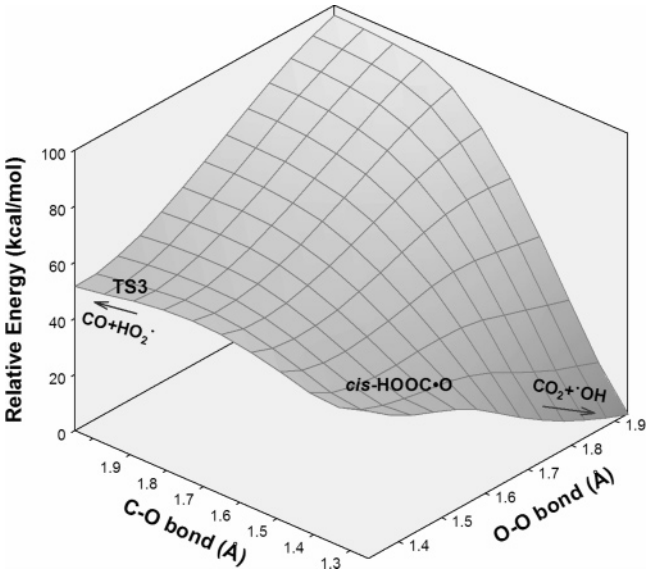

Figure 4. Relaxed potential energy scan at the B3LYP/6-31G(d) level of theory without zero-point correction, showing the reaction $(CO + HO_2\bullet) \rightarrow$ TS3 $\rightarrow CO_2 + \bullet OH$. *cis*-HOOC•O is represented by a local inflection point without a pronounced energy well.

The integration employed an energy spacing value equal to 1 cm^{-1}, which is sufficiently small to accurately compute $\rho(E)$ and $W(E)$ around the singularity point of $E = V_0$.[49]

Results and Discussion

The potential energy surface (PES) of reaction R1 is somewhat complicated by the existence of trans and cis conformers. At the B3LYP/6-31G(d) level of theory, a relaxed potential energy scan shows that *trans*-HOOC•O is a local minimum with two exit channels, one leading to $CO + HO_2\bullet$ (TS1) and the other leading to $CO_2 + \bullet OH$ (TS2), as seen in Figure 3. For *cis*-HOOC•O, a local minimum either does not exist or the potential energy well is too shallow to be of any importance. Figure 4 presents the companion potential energy scan for the cis configuration. Here the only saddle point corresponds to the direct $CO + HO_2\bullet \rightarrow CO_2 + \bullet OH$ reaction through TS3. The qualitative PES feature observed at the

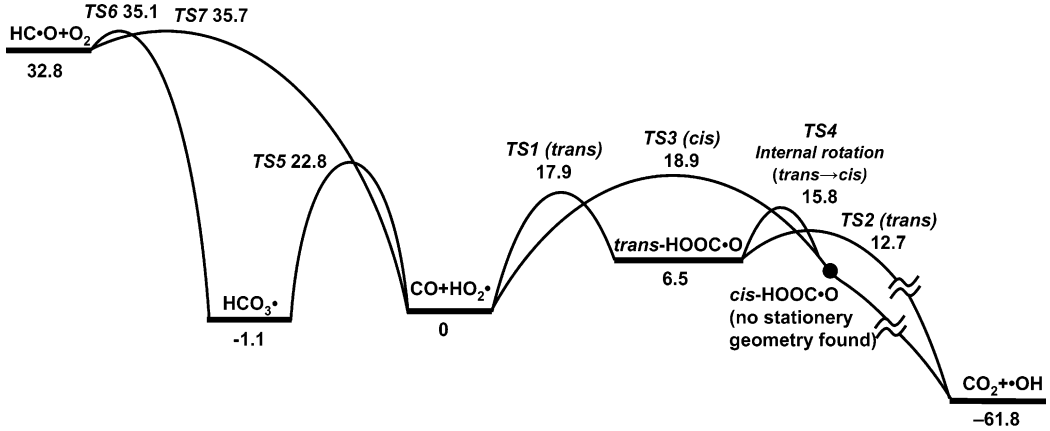

Figure 5. Potential energy diagram for CO + HO_2• → products. For CO + HO_2• → CO_2 + •OH, the energy values are determined using the CCSD(T)/CBS method, and include zero-point energy corrections. For CO + HO_2• → HC•O + O_2, the energy values are taken from Martínez-Ávila et al.[52] at QCISD(T)/6-311G(2df,2p)//QCISD/6-311G(d,p) level of theory.

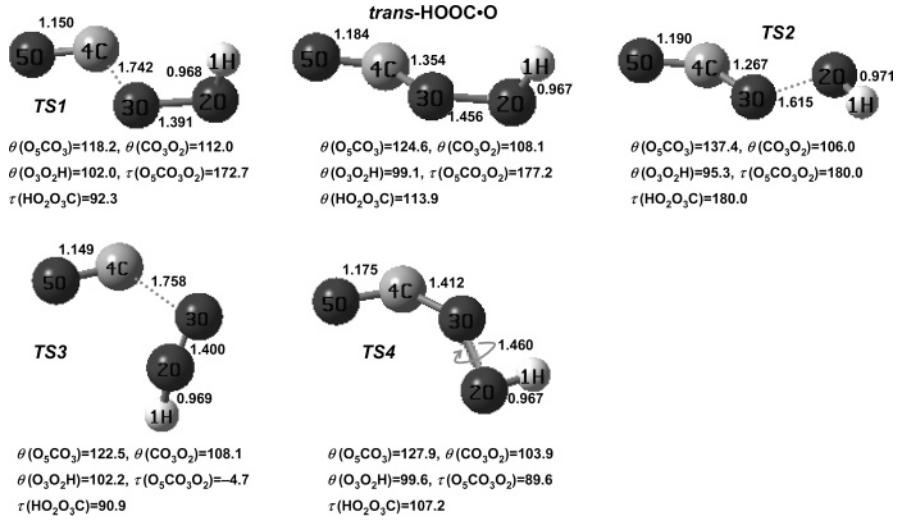

Figure 6. Geometry parameters determined at the CCSD(T)/cc-pVTZ level of theory. The bond lengths are in angstroms; and the bond and dihedral angles are in degrees.

TABLE 1: Energies (hartrees) Computed at Selected Levels of Theory

	G3B3	CCSD(T)/cc-pVTZ				CCSD(T)/ cc-pVQZ[c]	CCSD(T)/ CBS[d]	FCC/CBS[e]
species	E_0	E_0	T1 diag.	ZPE[a]	E^{T}[b]	E_0	E_0	E_0
O_2	−150.25273	−150.12904		0.00380	−0.01796	−150.17386	−150.20658	−150.21017
•OH	−75.69637	−75.63772		0.00853	−0.00510	−75.66163	−75.67908	−75.68010
CO	−113.26997	−113.15558		0.00491	−0.01714	−113.18787	−113.21143	−113.21485
CO_2	−188.50435	−188.32722		0.01183	−0.02875	−188.38452	−188.42633	−188.43208
HO_2•	−150.82995	−150.71272		0.01423	−0.01715	−150.75988	−150.79429	−150.79773
HC•O	−113.79409	−113.68411		0.01300	−0.01712	−113.71782	−113.74242	−113.74584
HOOC•O	−264.08981	−263.86006	0.020	0.02373	−0.03862	−263.94091	−263.99991	−264.00764
TS1	−264.07072	−263.84072	0.028	0.02147	−0.03904	−263.92096	−263.97951	−263.98732
TS2	−264.08075	−263.84751		0.02131	−0.04115	−263.92858	−263.98773	−263.99596
TS3	−264.06920	−263.83881	0.028	0.02129	−0.03984	−263.91913	−263.97774	−263.98571
TS4	−264.07527	−263.84451		0.02281	−0.03857	−263.92525	−263.98416	−263.99187

[a] Zero-point energy using the vibrational frequencies as calculated. For CO, CO_2, and •OH the average deviation of the vibrational frequencies from the experimental values is <1%, whereas for HO_2• the deviation is 4.5%. [b] The triple excitation $E^{T}_{\mathrm{CCSD(T)/cc-pVTZ}}$. [c] Single-point calculation at CCSD(T)/cc-pVTZ geometry. [d] See the text and eq 2. [e] See the text and eq 3.

B3LYP/6-31G(d) level of theory is consistent with calculations carried out using the CCSD(T)/cc-pVTZ method, though in the latter case only a limited PES scan was performed.

A schematic diagram illustrating the various stationary points along the trans and cis reaction pathways is provided in Figure 5. The corresponding CCSD(T)/cc-pVTZ geometry parameters are provided in Figure 6. These geometries are qualitatively similar to those obtained previously at the HF/6-31G(d) level of theory[35] for the trans conformer and its transition states.

TABLE 2: Energies (kcal/mol) at 0 K Relative to CO + HO_2•

products/ transition state	G3B3	CCSD(T)/ cc-pVTZ	CCSD(T)/ cc-pVQZ[a]	CCSD(T)/ CBS	FCC/CBS	literature value
CO_2 + •OH	−63.3	−59.9	−61.0	−61.8	−61.7	−61.6 ± 0.1
trans-HOOC•O	6.3	8.1	7.2	6.5	6.0	
TS1	18.3	18.8	18.3	17.9	17.3	
TS2	12.0	14.4	13.4	12.7	11.8	
TS3	19.3	19.9	19.3	18.9	18.2	
TS4	15.5	17.2	16.4	15.8	15.3	
HC•O + O_2	33.3	33.1	33.7	34.1	34.0	33.6 ± 0.1

[a] With CCSD(T)/cc-pVTZ zero-point energies.

TABLE 3: Literature Values of Enthalpy of Formation (kcal/mol)

species	$\Delta_f H_{298}$	$\Delta_f H_0$	ref/comments
•OH	8.9 ± 0.07	8.85	53
HO_2•	2.9 ± 0.1	3.6	54[a]
CO	−26.4 ± 0.04	−27.2	56[a]
CO_2	−94.1 ± 0.003	−94.0	56[a]
HC•O	10.1 ± 0.07	10.0	57

[a] $\Delta_f H_0$ values are obtained from $\Delta_f H_{298}$ and the sensible enthalpy values taken from ref 55.

Quantitatively, however, there are significant differences, with the CCSD(T)/cc-pVTZ O−O and O−C bond lengths being larger than the HF/6-31G(d) ones by as much as 0.1 Å.

Table 1 lists the absolute energies for the stationary points along these reaction pathways as computed using the semiempirical G3B3 method and for selected levels of single-reference theories. Here the CCSD(T)/cc-pVTZ energies were obtained from geometries optimized using the same method. The CCSD(T)/cc-pVQZ energies are the results of single-point calculations at the CCSD(T)/cc-pVTZ geometries. Energies extrapolated to the complete basis set (eq 2) are denoted as CCSD(T)/CBS, and those including the correction for the CI truncation error (eq 3) are denoted as FCC/CBS. The reaction enthalpies and energy barriers are presented in Table 2, where the literature values for the enthalpy of reaction are based on the heats of formation given in Table 3. Notably, both the CCSD(T)/CBS and FCC/CBS methods yield calculated reaction enthalpies within 0.5 kcal/mol of the literature value.

The CCSD(T)/CBS and FCC/CBS energy barriers are 17−18 kcal/mol for the addition of CO and HO_2• following the trans path (TS1) and around 18−19 kcal/mol following the cis path (TS3). Without basis-set extrapolation, these energy barriers are generally 0.5−1 kcal/mol larger than those with basis-set extrapolation. Interestingly, energy barriers predicted by the G3B3 method are within ∼1 kcal/mol of the CCSD(T)/CBS results, but this agreement may be fortuitous because the G3B3 enthalpy of reaction R1 is ∼2 kcal/mol lower than the literature value (see, Table 2). There are two pathways for *trans*-HOOC•O dissociation into CO_2 and •OH, as shown in Figure 5. The first path is a single O−O fission (TS2), and it requires only 6.2 kcal/mol of energy barrier. The second path involves trans → cis isomerization or internal rotation about HOO−C•O bond. Because *cis*-HOOC•O does not have a pronounced local energy minimum, the reaction path upon this isomerization collapses onto the cis pathway, as shown in Figure 5.

The T1 diagnostic computed for TS1 and TS3 casts some minor doubt on the reliability of the single-reference-based CCSD(T) correlation energies. For this reason, we have also explored the energetics of TS1 with CASPT2 and MRCI calculations, as reported in Table 4. The CASPT2 predictions of 18.2 and 18.4 kcal/mol for the TS1 barrier with the (9e,8o) and (11e,10o) active spaces are in good agreement with the CCSD(T)/CBS barrier of 17.9 kcal/mol, but are larger than the FCC/CBS barrier by about 1 kcal/mol. The somewhat lower value of 17.1 for the (5e,5o) active space is likely due to the importance of including the O−O π orbital in the active space. We have found it to be of similar importance in other related studies of radical + O_2 reactions. The MRCI calculations yield a much higher TS1 barrier of about 26 kcal/mol. The Davidson-corrected (CI+QC) TS1 barrier of about 21 kcal/mol is much closer to the CCSD(T) and CASPT2 values. It appears that the Davidson correction is qualitatively correct, but not quantitatively so. In related calculations for C_2H_4 + OH and for radical−radical abstraction reactions, we have similarly found that CASPT2 appears to provide a more consistent set of barriers[51] and that the Davidson correction is not quite as large as it needs to be. Thus, it appears reasonable to assume that the TS1 barrier is 17.9 kcal/mol, that is, an average among the barrier values from CCSD(T)/CBS, FCC/CBS, and CASPT2 with the (9e,8o) and (11e,10o) active spaces. The error bar on the energy barrier is expected to be ±1 kcal/mol, which corresponds to our experience for the typical uncertainty in CCSD(T) calculations of transition state energies and is also supported by the CASPT2 results. The CI and CI+QC calculations suggest that the upper error bar may be larger, but, importantly, there is no indication that the lower error bar should be any larger.

For comparison, the potential energies for the reaction

$$CO + HO_2\bullet \rightarrow HC\bullet O + O_2 \qquad \text{(R5)}$$

are also presented in Figure 5, based on QCISD(T)/6-311G

TABLE 4: Multireference Energies

		electronic energy (hartree)			critical energy (kcal/mol)		
geom. opt. (active space)	species	PT2/CBS	CI/CBS	CI+QC/CBS	PT2/CBS[a]	CI/CBS[a]	CI+QC/CBS[a]
PT2(5e,5o)	CO + HO_2•	−263.95871	−263.86127	−263.96559			
	TS1	−263.93363	−263.82223	−263.93379	17.1	25.9	21.3
PT2(9e,8o)	CO + HO_2•	−263.96020	−263.88270	−263.97633			
	TS1	−263.93333	−263.84389	−263.94445	18.2	25.7	21.4
PT2(11e,10o)	CO + HO_2•	−263.96211					
	TS1	−263.93497			18.4		

[a] With 1.38 kcal/mol zero-point energy correction from PT2(5e,5o)/atz.

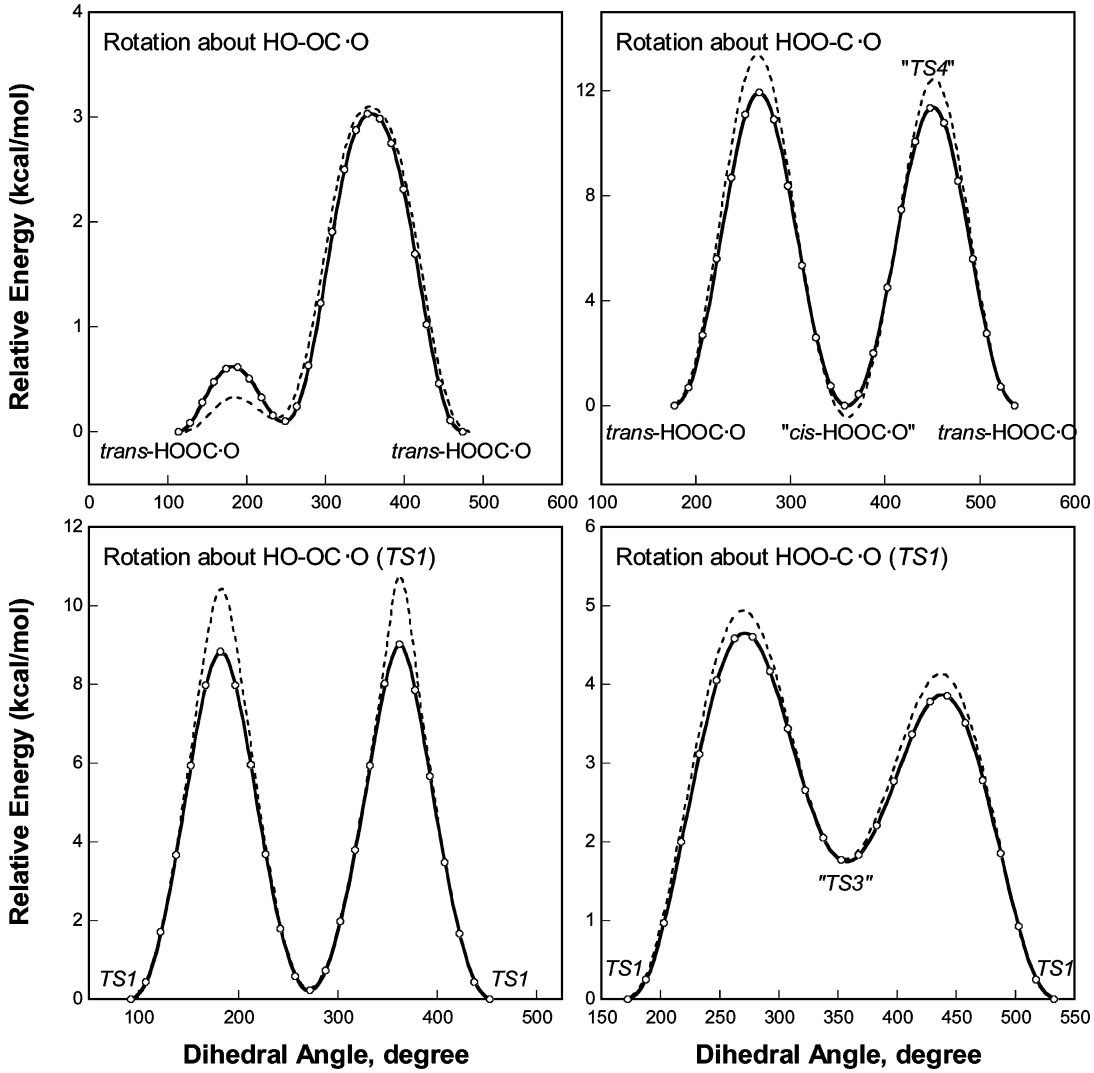

Figure 7. Energy scans for internal rotation in HOOC•O (top panels) and TS1 (bottom panels), computed at the CCSD(T)/cc-pVTZ (symbols and solid lines) and B3LYP/6-31G(d) (dotted lines) levels of theory. Except for the dihedral angle, geometries are frozen at those of *trans*-HOOC•O and TS1, respectively. Species/critical geometry given in quotes designates structures close to the respective optimized geometries.

(2df,2p)//QCISD/6-311G(d,p) results of Martínez-Ávila et al.[52] The formation of the HCO_3• adduct has an energy barrier around 23 kcal/mol, and the exit HC•O + O_2 channel has energy barriers around 35 kcal/mol. These barrier heights essentially rule out any importance of reaction R5 toward the total rate constant of CO + HO_2• → products.

The treatment of hindered internal rotation requires special consideration. The two rotors in question are those for rotating about the O−O and O−C bonds. The rotation about the O−C bond is responsible for the key trans-to-cis mutual isomerization. Figure 7 presents the potential energies for these two hindered internal rotations in HOOC•O and TS1. These potential energies were computed at the B3LYP/6-31G(d) and CCSD(T)/cc-pVTZ levels of theory. Except for the dihedral angle, the geometries are frozen during potential energy scans. Thus, the relative energies are expected to be somewhat larger than the true values. For example, the CCSD(T)/cc-pVTZ energy difference between TS3 and TS1 is 1.3 kcal/mol, whereas the rotation scan based on frozen geometries gives 1.8 kcal/mol (see the lower-right panel of Figure 7). These differences are considered in our assessment of the accuracy of the theoretical rate coefficient, as will be discussed later.

In the adduct, the rotational energy barrier for the HO−OC•O torsion is highly asymmetric, with barrier heights of roughly 0.6 and 3 kcal/mol. For the HOO−C•O torsion, the energy barrier is notably higher, being about 12 kcal/mol. In TS1, the HO−OC•O rotational barrier increases to about 9 kcal/mol, while the rotation about the HOO−C•O bond decreases to about 4 kcal/mol. The barrier heights calculated for TS3 are of a similar magnitude, as illustrated in Figure 8.

The absence of a potential minimum along the cis pathway suggests that it is best to treat the cis and trans reaction pathways separately. This separation is accomplished by excluding the contribution of the cis configuration to the partition function of the HOO−C•O hindered rotor for the trans pathway and vice versa for the trans configuration in the cis pathway. Specifically, the partition functions of HOO−C•O and TS1 were obtained by integrating over a rotation angle of $\phi = -\pi/2$ to $\pi/2$, or equivalently $0 < \phi \leq \pi/2$ and $3\pi/2 < \phi \leq 2\pi$. In other words, for these species the partition function given by eq 15 is truncated to only two terms

$$\rho_h(E) = \rho_{h1}(E) + \rho_{h4}(E) \tag{18}$$

Likewise, TS3, the transition state of CO + HO_2• on the cis pathway is treated by neglecting contributions from the trans part of the partition function. For the internal rotation about the HO−OC•O bond, the partition function is given by eq 15,

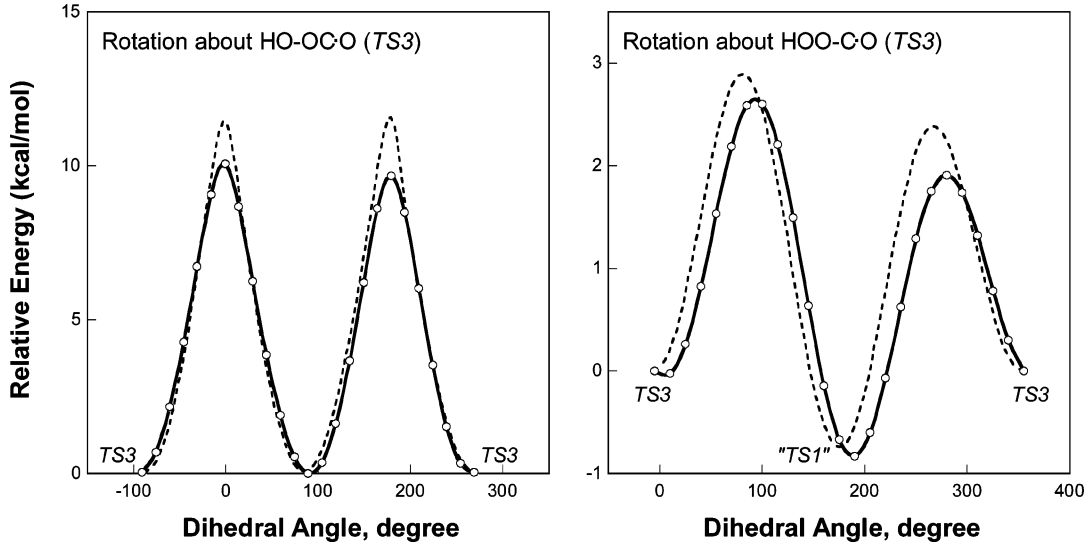

Figure 8. Energy scans for internal rotation in TS3, computed at the CCSD(T)/cc-pVTZ (symbols and solid lines) and B3LYP/6-31G(d) (dotted lines) levels of theory. Except for the dihedral angle, geometries are frozen at those of TS3. Critical geometry given in quotes designates a structure close to the optimized geometry.

TABLE 5: Molecular Properties Used for Computing the Rate Coefficient of CO + HO_2• → CO_2 + •OH

		B (cm^{-1})		hindered internal rotors[d]												
species	E_0[a] (kcal/mol)	inactive[b]	active[c]	mode	B (cm^{-1})	range	V_0[e] (kcal/mol)	ν (cm^{-1})[g]								
CO		1.91						2154								
HO_2•		20.5&1.1(2)						1135	1437	3674						
trans-HOOC•O	6.5	0.155	2.24	HO−OC•O	20.5	$0 < \phi \le \pi/2$	0.6	189[f]	249[f]	352	592	931	1047	1414	1861	3781
						$3\pi/2 < \phi \le 2\pi$	3.0									
						$\pi/2 < \phi \le \pi$	0.5									
						$\pi < \phi \le 3\pi/2$	2.9									
				HOO−C•O	4.1	$0 < \phi \le \pi/2$	11.4									
						$3\pi/2 < \phi \le 2\pi$	12.0									
TS1	17.9	0.133	1.89	HO−OC•O	20.8	$0 < \phi \le \pi/2$	8.8	661.1*i*	130[f]	265	417[f]	446	972	1429	2016	3748
						$3\pi/2 < \phi \le 2\pi$	9.0									
						$\pi/2 < \phi \le \pi$	8.6									
						$\pi < \phi \le 3\pi/2$	8.8									
				HOO−C•O	3.6	$0 < \phi \le \pi/2$	3.1									
						$3\pi/2 < \phi \le 2\pi$	3.8									
TS2	12.7	0.149	2.02	HO−OC•O	19.6	$0 < \phi \le 2\pi$	2.1	1535*i*	77[f]	322	343	784	928	1233	1916	3749
TS4	15.8	0.179	1.04	HO−OC•O	19.6	$0 < \phi \le \pi/2$	2.3	290*i*	290[f]	325	617	852	877	1380	1894	3776
						$3\pi/2 < \phi \le 2\pi$	7.4									
						$\pi/2 < \phi \le \pi$	2.0									
						$\pi < \phi \le 3\pi/2$	7.1									
TS3	18.9	0.172	0.77	HO−OC•O	19.5	$0 < \phi \le \pi/2$	9.6	705*i*	103[f]	224	467[f]	473	929	1400	2013	3736
						$3\pi/2 < \phi \le 2$	10.0									
						$\pi/2 < \phi \le \pi$	9.7									
						$\pi < \phi \le 3\pi/2$	10.1									
				HOO−C•O	6.5	$\pi/2 < \phi \le \pi$	2.1									
						$\pi < \phi \le 3\pi/2$	2.8									

[a] Relative to the energy of CO + HO_2• at 0 K. [b] With the exception of HO_2•, these are two-dimensional external inactive rotors (symmetry number $\sigma = 1$). [c] One-dimensional external rotors (symmetry number $\sigma = 1$). [d] One-dimensional hindered rotors (symmetry number $\sigma = 1$). [e] The energy barriers of hindered rotor V_0 (kcal/mol) are estimated from CCSD(T)/cc-pVTZ potential energy scan. [f] Vibrational mode replaced by hindered internal rotation. [g] From CCSD(T)/cc-pVTZ calculation (fully optimized geometry and numerical second derivatives).

where the asymmetric nature of the potential function is closely accounted for.

The internal rotational constants vary widely, depending on the level of approximation. For example, the B values for rotation about the HOO−C•O bond of *trans*-HOOC•O are 1.6, 14, and 4.1 cm^{-1} for $B^{(2,1)}$, $B^{(2,3)}$, and $B^{(3,4)}$, respectively. It is worth noting that the rotational constant is expected to be related to the force constant through the relation

$$B = \frac{\nu^2}{2(d^2V/d\phi^2)} \tag{19}$$

where ν is the vibrational frequency. Using the CCSD(T)/cc-pVTZ frequency value of 249 cm^{-1} and the potential energy shown in the upper-right panel of Figure 7, we obtain $B = 3.8$ cm^{-1}, which is in reasonably good agreement with the $B^{(3,4)}$ value. Furthermore, the $B^{(3,4)}$ value is the fundamentally most appropriate value and was thus adopted for all hindered internal rotations.

Table 5 lists the molecular parameters used in the rate calculation. Master equation modeling shows that, due to the shallow *trans*-HOOC•O potential energy well, there is no appreciable collisional stabilization of the rovibrationally excited *trans*-HOOC•O adduct for pressures up to 500 atm. Hence, for combustion applications the overall rate constant may be modeled as being independent of pressure. The *trans*-HOOC•O

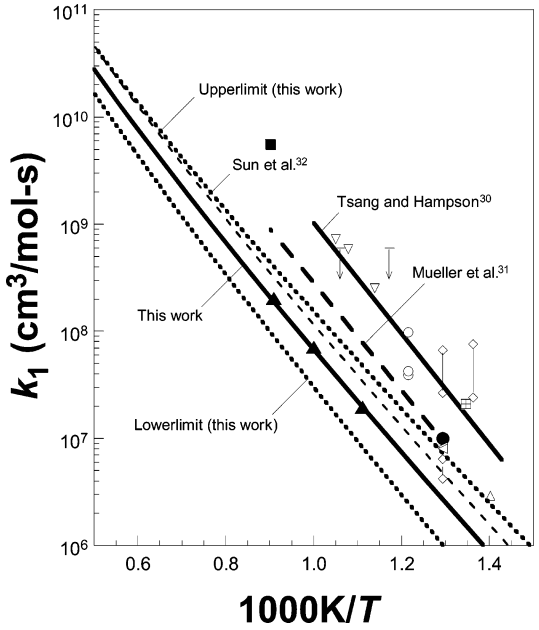

Figure 9. Experimental and theoretical rate coefficient for reaction R1. See the caption of Figure 1 for the source of the experimental data. The thick, dashed lines indicate the uncertainty bound of the current theoretical expression (see the text).

adduct has a finite, albeit short lifetime. At high temperatures, the overall rate constant through the trans pathway is influenced by the back dissociation to CO + HO_2•. The contribution of the trans pathway to the total rate coefficient is calculated to be

$$k_{1,\mathrm{trans}}(\mathrm{cm^3/mol{\cdot}s}) = 6.8 \times 10^5 T^{1.87} \mathrm{e}^{-8950/T}$$

over the temperature range of 300−2500 K.

Conventional transition state theory calculations yield a cis pathway contribution to the total rate coefficient of

$$k_{1,\mathrm{cis}}(\mathrm{cm^3/mol{\cdot}s}) = 2.2 \times 10^4 T^{2.39} \mathrm{e}^{-9260/T}$$

over the same temperature range. The trans pathway contributes 83, 55, and 42% of the total rate constant for $T = 300$, 1000, and 2000 K, respectively. As mentioned before, the decrease of the trans contribution with an increase in temperature is caused by the increasingly competitive dissociation of the rovibrationally excited *trans*-HOOC•O back to CO + HO_2• at higher temperatures.

The total pressure-independent rate coefficient, given as the sum of those for the two "channels", is

$$k_1(\mathrm{cm^3/mol{\cdot}s}) = 1.57 \times 10^5 T^{2.18} \mathrm{e}^{-9030/T} \quad \text{for } 300 \le T \le 2500 \text{ K} \quad (20)$$

where the fitting error is less than 5% over the entire range of temperature.

Figure 1 shows a comparison of the current theoretical predictions for the rate coefficient with previous studies and evaluations. The same Arrhenius plot is shown over a narrower temperature region in Figure 9. Clearly the current analysis supports the lower k_1 values based on the RCM analysis of Mittal et al.[1,2] Quantitatively, our k_1 expression is within 10% of the expression of Mittal et al. over the temperature range of 950−1100 K. Although this close agreement may be fortuitous, the current results, obtained from very high-level quantum chemistry calculation and master equation modeling with a careful treatment of internal rotations clearly supports the notion advanced in these RCM studies that the literature rate values for k_1 are too large.

TABLE 6: Effect of Internal Rotor Treatments on k_1 (cm^3/mol·s)

			hindered rotor		
T (K)	harmonic oscillator	free rotor with $I^{(3,4)}$	$I^{(2,1)}$	$I^{(2,3)}$	$I^{(3,4)a}$
500	2.1×10^3	3.8×10^4	2.9×10^3	1.5×10^3	1.7×10^3
1000	5.6×10^7	6.1×10^8	1.1×10^8	6.3×10^7	6.5×10^7
1500	2.6×10^9	2.1×10^{10}	5.5×10^9	3.4×10^9	3.2×10^9
2000	2.2×10^{10}	1.4×10^{11}	4.7×10^{10}	2.9×10^{10}	2.7×10^{10}
2500	8.8×10^{10}	4.6×10^{11}	1.9×10^{11}	1.2×10^{11}	1.1×10^{11}

[a] Theory with which the final theoretical rate constant was computed.

To illustrate the need to properly treat the hindered internal rotors and their reduced moments of inertia, we present in Table 6 k_1 values obtained at several levels of theoretical approximation. As expected, the limiting case of the free-rotor treatment (with $I^{(3,4)}$) yields k_1 values substantially larger than those of the harmonic oscillator treatment, by approximately a factor of 10. The different treatments for the reduced moment inertia can lead to an uncertainty of a factor of ∼2. In particular, rate constants from $I^{(2,1)}$ are a factor of ∼2 larger than those from $I^{(3,4)}$. Thus, the combined uncertainty is expected to be a factor of 20, which underscores the need for an accurate treatment of the hindered internal rotor.

The hindered rotor approach gives k_1 values much closer to the harmonic oscillator than to free rotor, but the close agreement between hindered rotor and harmonic oscillator treatments is fortuitous at best because the relevant vibrational frequencies are generally <150 cm^{-1}, and thus the harmonic approximation for these otherwise anharmonic oscillators are dubious at best. An important point here is that without a careful treatment of the hindered rotors the uncertainty in the theoretical rate constant is as large as the scatter in the experimental data shown in Figure 1, and even more importantly the true uncertainty in the theoretical k_1 cannot be quantified.

Our earlier discussion placed an uncertainty bar of ±1 kcal/mol on the reaction energy barriers. Sensitivity tests showed that k_1 is the most sensitive to the energy values of TS1 and TS3, and the energy barriers of internal rotation between TS1 and TS3. Assuming that all of these barrier values are accurate to within ±1 kcal/mol, plus an additional, temperature-independent uncertainty of 50% in state counting, we obtained the theoretical upper and lower limits for k_1, as shown by the thick, dashed lines in Figure 9. The corresponding uncertainty factors are about 8, 2, and 1.7 for temperatures of 300, 1000, and 2000 K.

Almost all earlier experimental rate values may now be rejected in light of the current analysis. An inspection of Figure 9 shows that the measurements reported by Baldwin and coworkers[4,6,16] fall above the upper bound of the current theoretical results. In addition, the k_1 expression of Mueller et al.[31] is close, but above our upper limit, whereas the rate values of Sun et al.[32] are within our uncertainty bounds, despite the fact that only the trans configuration was considered in their analysis.

It is worth noting that the rate coefficient for the second channel (reaction R5) is substantially smaller than the current theoretical k_1 value. k_5 values may be estimated from the rate coefficient of the back reaction[36] to be 3×10^5 and 2×10^9 cm^3/mol·s at 1000 and 2000 K, respectively, which are no larger than 10% of k_1, as expected from the potential energy differences of reactions R1 and R5, as seen in Figure 5.

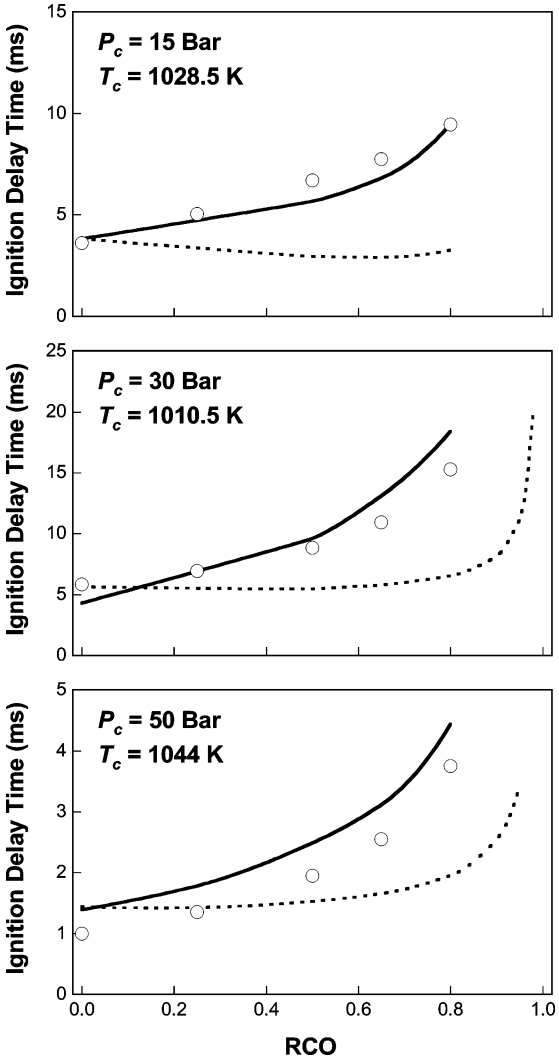

Figure 10. Predictions of RCM ignition delay times at compressed pressures P_c = 15, 30 and 50 bar, and compressed temperatures T_c around 1020 K. Molar composition: $(H_2 + CO)/O_2/N_2/Ar = 12.5/6.25/18.125/63.125$. RCO is defined as the molar concentration ratio [CO]/([H_2] + [CO]). Solid lines, updated model of Davis et al.[58] (see the text); dashed line, original model.

We examined the accuracy of a previously proposed H_2/CO oxidation model[58] by updating only three rate coefficients: k_1 based on the current study, the rate coefficient of CO + •OH → CO_2 + H• from Joshi and Wang,[27] and k_2 evaluated in Sivaramakrishnan et al.[3] Figure 10 shows the comparison of experimental and computed ignition delays for RCM experiments at 15, 30, and 50 atm, before and after these updates. Here, RCO is defined as the mole fraction of CO in the combined H_2/CO fuel mixture. In simulating RCM experiments, effects of compression stroke and heat loss are included.[1] In all cases, an increase in the CO concentration in the unburned mixture increases the ignition delay time. It is seen that the updates just discussed led to drastic improvement of the predictions, as expected. The improvement was brought almost entirely from the revision of the rate coefficient of reaction R1. In addition, the same reaction model was tested against the single-pulse shock-tube experiments of H_2/CO oxidation up to 500 bar.[3] The comparison (not shown here) is satisfactory.

Since this paper was completed, another study of the PES and rate constant of reaction R1 was presented at a recent conference.[59] That study included a broad analysis of the PES but employed considerably lower-level quantum chemistry methods (CBS/QB3, CCSD(T)/6-311+G(d,p)//B3LYP/6-311G(d,p), and CBS-APNO) and focused on only the trans pathway. The resulting predictions for the energy barrier for the CO + HO_2 addition ranged from 15.4 to 19 kcal/mol. Furthermore, the QRRK approach employed in their kinetic analysis is perhaps not the best choice to obtain accurate rate coefficients. The net result is that the predicted k_1 value of ref 59 is substantially larger, by an order of magnitude, than the k_1 value reported here. This difference is attributable, to a small extent, to the difference in the energy barrier of the two studies. A larger part of the difference likely arises from the QRRK treatments of vibrational frequencies from the B3LYP basis of that vibrational frequeny analysis and a lack of the treatment of hindered internal rotation. The above discussion applies equally to the theoretical studies of Sun et al.[32] and Hsu et al.[36] In both cases, these authors considered only the trans pathway and employed considerably lower-level quantum chemical and reaction rate theory methods than the present study.

Last, we note that despite the arguments made above the validity of our theoretical results are yet to be proved by well-defined kinetic measurement. In comparison to other theoretical studies, however, the unique contribution of the present work is that it provides a test case for the highest levels of quantum chemistry methods and rate theory suitable for this type of reaction.

Conclusions

The reaction kinetics of CO + HO_2• → CO_2 + •OH (R1) was studied using the single-reference CCSD(T) method with Dunning's cc-pVTZ and cc-pVQZ basis sets and multireference CASPT2 methods. It was found that the classical energy barriers are about 18 and 19 kcal/mol for CO + HO_2• addition following the trans and cis paths. The HOOC•O adduct has a well-defined local energy minimum in the trans configuration, but the cis conformer is either a very shallow minimum or an inflection point on the potential energy surface. This observation led us to treat the cis pathway with conventional transition state theory and the trans pathway with a master equation analysis. The computation shows that the overall rate is independent of pressure up to 500 atm. Upon a careful treatment of the hindered internal rotations in the HOOC•O adduct and relevant transition states, we obtain a rate coefficient expression $k_1(cm^3/mol{\cdot}s) = 1.57 \times 10^5 T^{2.18} e^{-9030/T}$ for $300 \le T \le 2500$ K. This rate expression is within 10% of that of Mittal et al.,[1] obtained on the basis of an analysis of RCM experiments of H_2/CO oxidation in the temperature range of 950−1100 K. Considering the underlying uncertainties in the theoretical energy barriers, we carried out a parameter sensitivity analysis for k_1 and estimated the uncertainty factor for the theoretical expression to be 8, 2, and 1.7 at temperatures of 300, 1000, and 2000 K, respectively. These error bars reject almost all of the rate values reported in earlier studies, with the exception of Mittal et al.[1,2]

Acknowledgment. The work was partially sponsored by the U.S. Department of Energy (Grant No. DE-FG26-06NT42717) (H.W. and C.-J.S.), by the U.S. Air Force Office of Scientific Research AFOSR (Grant No. FA9550-05-1-0010) (H.W.), and by the Office of Basic Energy Sciences, Division of Chemical Sciences, Geosciences, and Biosciences, U.S. Department of Energy, under contract no. DE-AC02-06CH11357 (S.J.K.). E.G. thanks DLR for a three-month research award. We thank G. Mittal for his help in RCM calculations.

References and Notes

(1) Mittal, G.; Sung, C. J.; Yetter, R. *Int. J. Chem. Kinet.* **2006**, *38*, 516.

(2) Mittal, G.; Sung, C. J.; Fairweather, M.; Tomlin, A. S.; Griffiths, J. F.; Hughes, K. J. *Proc. Combust. Inst.* **2007**, *31*, 419.
(3) Sivaramakrishnan, R.; Comandini, A.; Tranter, R. S.; Brezinsky, K.; Davis, S. G.; Wang, H. *Proc. Combust. Inst.* **2007**, *31*, 429.
(4) Baldwin, R. R.; Jackson, D.; Walker, R. W.; Webster, S. J. *Proc. Combust. Inst.* **1965**, *10*, 423.
(5) Hoare, D. E.; Patel, M. *Trans. Faraday Soc.* **1969**, *65*, 1325.
(6) Baldwin, R. R.; Walker, R. W.; Webster, S. J. *Combust. Flame* **1970**, *15*, 167.
(7) Azatyan, V. V. *Dokl. Akad. Nauk. SSSR* **1971**, *196*, 617.
(8) Volman, D. H.; Gorse, R. A. *J. Phys. Chem.* **1972**, *76*, 3301.
(9) (a) Westenberg, A. A. *Science* **1972**, *177*, 255. (b) Westenberg, A.A.; de Haas, N. *J. Phys. Chem.* **1972**, *76*, 1586.
(10) Khachatrian, M. S.; Azatian, V. V.; Parsamian, N. I. *Arm. Khim. Zh.* **1972**, *25*, 367.
(11) Davis, D. D.; Payne, W. A.; Stief, L. J. *Science* **1973**, *179*, 280.
(12) Simonaitis, R.; Heicklen, J. *J. Phys. Chem.* **1973**, *77*, 1096.
(13) Wyrsch, D.; Wendt, H. R.; Hunziker, H. E. *Berichte Bunsen-Ges.* **1974**, *78*, 204.
(14) Hastie, J. W. *Chem. Phys. Lett.* **1974**, *26*, 338.
(15) Vardanyan, I. A.; Sachyan, G. A.; Nalbandyan, A. B. *Int. J. Chem. Kinet.* **1975**, *7*, 23.
(16) Atri, G. M.; Baldwin, R. R.; Jackson, D.; Walker, R. W. *Combust. Flame* **1977**, *30*, 1.
(17) Colket, M. B., III.; Naegeli, D. W.; Glassman, I. *Proc. Combust. Inst.* **1977**, *16*, 1023.
(18) Graham, R. A.; Winer, A. M.; Atkinson, R.; Pitts, J. N., Jr. *J. Phys. Chem.* **1979**, *83*, 1563.
(19) Burrow, J. P.; Cliff, D. I.; Harris, G. W.; Thrush, B. A.; Wilkinson, F. R. S.; Wilkinson, J. P. T. *Proc. R. Soc. London, Ser. A* **1979**, *368*, 463.
(20) Howard, C. J. *J. Chem. Phys.* **1979**, *71*, 2352.
(21) Arustamyan, A. M.; Shakhnazaryan, I. K.; Philipossyan, A. G.; Nalbandyan, A. B. *Int. J. Chem. Kinet.* **1980**, *12*, 55.
(22) Vandooren, J.; Oldenhove de Guertechin, L.; van Tiggelen, P. J. *Combust. Flame* **1986**, *64*, 127.
(23) Bohn, B.; Zetsch, C. *J. Chem. Soc. Faraday Trans.* **1998**, *94*, 1203.
(24) Kappel, Ch.; Luther, K.; Troe, J. *Phys. Chem. Chem. Phys.* **2002**, *4*, 4392.
(25) Baulch, D. L.; Bowman, C. T.; Cobos, C. J.; Cox, R. A.; Just, Th.; Kerr, J. A.; Pilling, M. J.; Stocker, D.; Troe, J.; Tsang, W.; Walker, R. W.; Warnatz, J. *J. Phys. Chem. Ref. Data* **2005**, *34*, 757.
(26) Baldwin, R. R.; Dean, C. E.; Honeyman, M. R.; Walker, R. W. *J. Chem. Soc. Faraday Trans. 1* **1986**, *82*, 89.
(27) Joshi, A. V.; Wang, H. *Int. J. Chem. Kinet.* **2006**, *38*, 57.
(28) Atkinson, R.; Baulch, D. L.; Cox, R. A.; Crowley, J. N.; Hampson, R. F.; Hynes, R. G.; Jenkin, M. E.; Rossi, M. J.; Troe, J. *Atmos. Chem. Phys.* **2004**, *4*, 1461.
(29) Lloyd, A. C. *Int. J. Chem. Kinet.* **1974**, *6*, 169.
(30) Tsang, W.; Hampson, R. F. *J. Phys. Chem. Ref. Data* **1986**, *15*, 1087.
(31) Mueller, M. A.; Yetter, R. A.; Dryer, F. L. *Int. J. Chem. Kinet.* **1999**, *31*, 705.
(32) Sun, H. Y.; Yang, S. I.; Jomaas, G.; Law, C. K. *Proc. Combust. Inst.* **2007**, *31*, 439.
(33) Hippler, H.; Troe, J.; Willner, J. *J. Chem. Phys.* **1990**, *93*, 1755.
(34) Zarubiak, D. C. Z. M.S. Thesis, Department of Mechanical and Aerospace Engineering, Princeton University, Princeton, NJ, 1997.
(35) Allen, T. L.; Fink, W. H.; Volman, D. H. *J. Phys. Chem.* **1996**, *100*, 5299.
(36) Hsu, C. C.; Mebel, A. M.; Lin, M. C. *J. Chem. Phys.* **1996**, *105*, 2346.
(37) Woon, D. E.; Dunning, T. H., Jr. *J. Chem. Phys.* **1993**, *98*, 1358.
(38) Frisch, M. J.; Trucks, G. W.; Schlegel, H. B.; Scuseria, G. E.; Robb, M. A.; Cheeseman, J. R.; Montgomery, J. A., Jr.; Vreven, T.; Kudin, K. N.; Burant, J. C.; Millam, J. M.; Iyengar, S. S.; Tomasi, J.; Barone, V.; Mennucci, B.; Cossi, M.; Scalmani, G.; Rega, N.; Petersson, G. A.; Nakatsuji, H.; Hada, M.; Ehara, M.; Toyota, K.; Fukuda, R.; Hasegawa, J.; Ishida, M.; Nakajima, T.; Honda, Y.; Kitao, O.; Nakai, H.; Klene, M.; Li, X.; Knox, J. E.; Hratchian, H. P.; Cross, J. B.; Bakken, V.; Adamo, C.; Jaramillo, J.; Gomperts, R.; Stratmann, R. E.; Yazyev, O.; Austin, A. J.; Cammi, R.; Pomelli, C.; Ochterski, J. W.; Ayala, P. Y.; Morokuma, K.; Voth, G. A.; Salvador, P.; Dannenberg, J. J.; Zakrzewski, V. G.; Dapprich, S.; Daniels, A. D.; Strain, M. C.; Farkas, O.; Malick, D. K.; Rabuck, A. D.; Raghavachari, K.; Foresman, J. B.; Ortiz, J. V.; Cui, Q.; Baboul, A. G.; Clifford, S.; Cioslowski, J.; Stefanov, B. B.; Liu, G.; Liashenko, A.; Piskorz, P.; Komaromi, I.; Martin, R. L.; Fox, D. J.; Keith, T.; Al-Laham, M. A.; Peng, C. Y.; Nanayakkara, A.; Challacombe, M.; Gill, P. M. W.; Johnson, B.; Chen, W.; Wong, M. W.; Gonzalez, C.; Pople, J. A. *Gaussian 03*, revision C.02; Gaussian, Inc.: Wallingford, CT, 2004.
(39) Halkier, A.; Helgaker, T.; Jorgensen, P.; Klopper, W.; Koch, H.; Olsen, J.; Wilson, A. K. *Chem. Phys. Lett.* **1998**, *286*, 243.
(40) He, Y.; He, Z.; Cremer, D. *Chem. Phys. Lett.* **2000**, *317*, 535.
(41) Yu, H.-G.; Muckerman, J. T.; Sears, T. J. *Chem. Phys. Lett.* **2001**, *349*, 547.
(42) Lee, T. J.; Rendell, A. P.; Taylor, P. R. *J. Phys. Chem.* **1990**, *94*, 5463.
(43) Lee, T. J.; Taylor, P. R. *Int. J. Quantum Chem., Quantum Chem. Symp.* **1989**, *23*, 199.
(44) (a) Werner, H.-J. *Mol. Phys.* **1996**, *89*, 645. (b) Celani, P.; Werner, H.-J. *J. Chem. Phys.* **2000**, *112*, 5546.
(45) *MOLPRO* is a package of ab initio programs written by Werner, H.-J.; Knowles, P. J. with contributions from Almlof, J.; Amos, R. D.; Berning, A.; Cooper, D. L.; Deegan, M. J. O.; Dobbyn, A. J.; Eckert, F.; Elbert, S. T.; Hampel, C.; Lindh, R.; Lloyd, A. W.; Meyer, W.; Nicklass, A.; Peterson, K.; Pitzer, R.; Stone, A. J.; Taylor, P. R.; Mura, M. E.; Pulay, P.; Schutz, M.; Stoll, H.; Thorsteinsson, T.
(46) East, A. L. L.; Radom, L. *J. Chem. Phys.* **1997**, *106*, 6655.
(47) Gilbert, R. G.; Smith, S. C. *Theory of Unimolecular and Recombination Reactions*; Blackwell: Oxford, 1990.
(48) Pitzer, K. S. *J. Chem. Phys.* **1946**, *14*, 239.
(49) Knyazev, V. D.; Dubinsky, I. A.; Slagle, I. R.; Gutman, D. *J. Phys. Chem.* **1994**, *98*, 5279.
(50) Knyazev, V. D.; Tsang, W. *J. Phys. Chem. A* **1998**, *102*, 9167.
(51) Klippenstein, S. J.; Harding, L. B. Unpublished results.
(52) Martínez-Ávila, M.; Peiró-García, J.; Ramírez-Ramírez, V. M.; Nebot-Gil, I. *J. Chem. Phys.* **2003**, *370*, 313.
(53) Ruscic, B.; Wagner, A. F.; Harding, L. B.; Asher, R. L.; Feller, D.; Dixon, D. A.; Peterson, K. A.; Song, Y.; Qian, X.; Ng, C.-Y.; Liu, J.; Chen, W.; Schwenke, D. W. *J. Phys. Chem. A* **2002**, *106*, 2727.
(54) Ruscic, B.; Pinzon, R. E.; Morton, M. L.; Srinivasan, N. K.; Su, M.-C.; Sutherland, J. W.; Michael, J. V. *J. Phys. Chem. A* **2006**, *110*, 6592.
(55) Chase, M. W., Jr. *J. Phys. Chem. Ref. Data, Monogr. 9* **1998**.
(56) Burcat, A.; Ruscic, B. *Third Millennium Ideal Gas and Condensed Phase Thermodynamical Database for Combustion with Updates from Active Thermochemical Tables*, ANL-05/20 and TAE 960 Technion-IIT, Aerospace Engineering, and Argonne National Laboratory, Chemistry Division, September 2005.
(57) Marenich, A. V.; Boggs, J. E. *J. Phys. Chem. A* **2003**, *107*, 2343.
(58) Davis, S. G.; Joshi, A. V.; Wang, H.; Egolfopoulos, F. N. *Proc. Combust. Inst.* **2005**, *30*, 1283.
(59) Asatryan, R.; Rutz, L.; Bockhorn, H.; Bozzelli, J. Computational Thermochemistry and Kinetics for the HO_2 + CO Reaction. International Workshop on Gas Kinetics, Sonderforschungsbereich SFB 606, 17 November 2006, Karlsruhe, Germany.